KDM2B promotes cell viability by enhancing DNA damage response in canine hemangiosarcoma

Kevin Christian M. Gulay[1], Keisuke Aoshima[1*], Yuki Shibata[2], Hironobu Yasui[2], Qin Yan[3], Atsushi Kobayashi[1] & Takashi Kimura[1]

[1] Laboratory of Comparative Pathology, Department of Clinical Sciences, Faculty of Veterinary Medicine, Hokkaido University, Sapporo, Hokkaido, 060-0818, Japan.

[2] Laboratory of Radiation Biology, Department of Applied Veterinary Sciences, Faculty of Veterinary Medicine, Hokkaido University, Sapporo, Hokkaido, 060-0818, Japan.

[3] Department of Pathology, Yale School of Medicine, New Haven, CT, USA.

*Correspondence to Keisuke Aoshima, Laboratory of Comparative Pathology, Department of Clinical Veterinary Sciences, Faculty of Veterinary Medicine, Hokkaido University, Kita 18 Nishi 9, Kita-ku, Sapporo, Hokkaido 060-0818, Japan: k-aoshima@vetmed.hokudai.ac.jp: Tel. +81-11-706-5193

Abstract

Epigenetic regulators have been implicated in tumorigenesis of many types of cancer; however, their roles in endothelial cell cancers such as canine hemangiosarcoma (HSA) have not been studied. In this study, we found that lysine-specific demethylase 2B (Kdm2b) was highly expressed in HSA cell lines compared to normal canine endothelial cells. Silencing of Kdm2b in HSA cells resulted to increased cell death *in vitro* compared to the scramble control by inducing apoptosis through the inactivation of the DNA repair pathways and accumulation of DNA damage. Similarly, doxycycline-induced Kdm2b silencing in tumor xenografts resulted to decreased tumor sizes compared to the scramble control. Furthermore, Kdm2b was also highly expressed in clinical cases of HSA, and its expression levels was higher than in hemangioma, a benign counterpart of HSA. Based on these results, we hypothesized that pharmacological Kdm2b inhibition can also induce HSA cell death and can be used as an alternative treatment for HSA. We treated HSA cells with GSK-J4, a histone demethylase inhibitor, and found that GSK-J4 treatment also induced apoptosis and cell death. On top of that, GSK-J4 treatment in HSA tumor-bearing mice decreased tumor sizes without any obvious side-effects. In this study, we demonstrated that Kdm2b acts as an oncogene in HSA by enhancing DNA damage response and can be used as a biomarker to differentiate HSA from hemangioma. Moreover, we indicated that histone demethylase inhibitor GSK-J4 can be used as a therapeutic alternative to doxorubicin for HSA treatment.

Keywords

DNA repair, epigenetics, hemangiosarcoma, KDM2B, oncogene

Introduction

Canine hemangiosarcoma (HSA) is a highly malignant tumor of vascular endothelial cells. It is an aggressive tumor with high rates of local recurrence and metastasis, and a low overall survival time[1]. Its high cellular heterogeneity has limited genomic and pathogenesis studies in HSA. Genomic analyses have revealed that HSA cells have somatic coding mutations in the *TP53*, *PIK3CA*, and *PIK3R1*. Furthermore, *CDKN2A*/B were found to be consistently deleted and copies of *VEGFA*, *KDR* and *KIT* were gained[2]. The oncogene involved in HSA, however, is still unknown.

Epigenetic mechanisms are essential for reproduction, embryonic development, and maintenance of normal cell function in eukaryotes[3]. Generally, the genetic alterations that cause tumorigenesis are combined with epigenetic shifts, such as aberrant DNA methylation and histone modifications, which may help oncogenic drivers improve cancer development, metastasis, and resistance to therapies[4]. KDM2B (also known as NDY1 and FBXL10), an H3K4me3, H3K36me2/3 and H3K79me3 demethylase, acts as a tumor suppressor in gastric cancer by downregulating glycolysis, and tumor-derived mutation in Kdm2b enhances cell proliferation through the inability of c-FOS degradation[5]. Alternatively, KDM2B can also act as an oncogene in various types of cancers. In leukemia, Kdm2b is highly expressed and is sufficient to transform hematopoietic progenitor cells[6]. In breast cancer, KDM2B regulates

polycomb complexes and controls self-renewal of breast cancer stem cells[7]. This bifunctional activity means that the role of KDM2B in tumors is highly context dependent and must be evaluated carefully[8]. While epigenetics is highly involved in pathogenesis of many cancers, its role in HSA is still unknown.

Treatment of HSA is carried out by tumor excision and chemotherapy with doxorubicin, cisplatin, or 5-fluorouracil[9,10]. The mean survival time for surgical treatment is 3 months while the mean survival time for surgical treatment with chemotherapy is less than a year[11,12]. Chemotherapeutic drugs fail to improve survival times of cancer patients due to the non-specificity of their cytotoxic effects in the cardiomyocytes, brain, liver and intestine[13,14]. A more effective, specific, and safer treatment for HSA is warranted.

Histone demethylase inhibitors are effective agents for anticancer treatment. In a previous study, GSK-J4, a histone demethylase inhibitor, decreased AML disease progression by downregulating DNA replication and cell cycle-related pathways through the enrichment of H3K27me3[15]. GSK-J4 was initially developed as a KDM6 inhibitor, but it was found to inhibit the catalytic activity of a wide range of JmjC domain-containing histone demethylases including KDM2B[16]. Epigenetic therapy may provide additional treatment option, but no epigenetic drug has tested for HSA.

In this study, we sought to establish the pathogenesis and to find a therapeutic

alternative for HSA by examining the role of epigenetic regulators.

Results

Kdm2b is important for HSA cell survival

We first performed RNA-sequencing analysis of canine aortic endothelial cells (CnAOEC) and one HSA cell line, JuB2, to examine the expression levels of epigenetic modifiers. Among the differentially expressed genes, histone methyltransferases/demethylases, histone acetyltransferases/deacetylases, and DNA methyltransferase/demethylases were dysregulated in JuB2 compared to CnAOEC (Fig. 1A, Supplementary Fig. 1A). Next, we performed qRT-PCR to verify RNA-seq results of histone methyltransferases/demethylases in CnAOEC and seven HSA cell lines. Some histone methyltransferases were incoherently expressed in HSA cell lines compared to CnAOEC (Supplementary Fig. 1B). In contrast, three histone demethylases were significantly upregulated in HSA cells compared to CnAOEC. Moreover, one set of paralogs (*KDM2A* and *KDM2B*) were enriched, which implies their importance in HSA (Fig. 1B). We then performed western blotting for Kdm1a, Kdm2a, and Kdm2b and found that their protein levels were upregulated in all HSA cell lines compared to CnAOEC (Fig. 1C and D). To provide further evidence, we performed qRT-PCR analysis in ISO-HAS-B, a human angiosarcoma cell line, compared to Human Umbilical Vein Endothelial

Cells (HUVEC). We revealed that histone methyltransferases/demethylases were also dysregulated in ISO-HAS-B (Supplementary Fig. 1C and Fig. 1E). Furthermore, protein expression levels of KDM1A, KDM2A and KDM2B were also upregulated in ISO-HAS-B compared to HUVEC (Fig. 1F and G). These results suggest that epigenetic regulators, specifically Kdm1a, Kdm2a, and Kdm2b, are highly expressed in HSA and human angiosarcoma and, thus, may have a significant role in endothelial cell tumors.

To examine whether the overexpression of Kdm1a, Kdm2a and Kdm2b has important functional roles in HSA, we designed three shRNA sequences for each gene to knockdown *KDM1A*, *KDM2A* and *KDM2B* as well as two scramble RNA controls (scrRNA), and we expressed these shRNAs in HSA cell lines using a doxycycline (Dox)-inducible vector system. Knockdown was verified with western blotting after four days of Dox treatment (Fig. 2A)**.** Knockdown of *KDM1A* and *KDM2A* did not have short term effects in JuB2 viability, whereas knockdown of *KDM2B* markedly decreased JuB2 viability within 4 days (Fig. 2B). To evaluate long term effects of Kdm1a, Kdm2a and Kdm2b on JuB2 cell survival, we performed colony formation assay and found that *KDM1A* and *KDM2A* knockdown could inhibit JuB2 colony formation, whereas *KDM2B* knockdown significantly reduced the number of colonies of JuB2 (Fig. 2C and D, Supplementary Fig. 2A and B). Kdm2b knockdown with constitutively expressed shRNA vectors also induced the same phenotype in JuB2 cells and other HSA cell

lines such as JuB4, Re21, and Ud6 (Supplementary Fig. 2C and D). These results suggest that Kdm2b is an important histone demethylase in HSA cell survival, which encouraged us to further investigate its function. To examine whether Kdm2b can alter overall histone methylation levels in HSA, we performed western blotting for histone methylations that can be modified by Kdm2b. However, all possible histone methylations were not affected in JuB2 after *KDM2B* knockdown (Supplementary Fig. 2E). Next, to investigate which Kdm2b domain is responsible for HSA cell viability, we rescued Kdm2b function in *KDM2B* silenced HSA cells. We expressed wild type (WT) canine Kdm2b with silent mutations for the sequences which were targeted by the shRNAs and Kdm2b mutants with a point mutation for the JmjC domain (Kdm2b^{H283Y}), the CXXC domain (Kdm2b^{C586A}), or with PHD-finger domain deleted (Kdm2b$^{\triangle PHD}$)[17–19]. Overexpression of WT Kdm2b and Kdm2b^{C586A} mutant but not the Kdm2b^{H283Y} or the Kdm2b$^{\triangle PHD}$ mutants rescued the phenotype (Fig. 2E), which suggests that the JmjC and the PHD-finger domains are important for the Kdm2b function in HSA.

To verify our *in vitro* results and to know the effect of Kdm2b silencing *in vivo*, JuB2 cells with Dox-inducible shRNAs against *KDM2B* or the scramble shRNA were injected subcutaneously into nude mice and the tumor volumes over time were measured. Dox-containing food pellets were provided to the mice to induce shRNA expression when the largest tumor reached 150 mm^3 in volume. Tumor xenografts started to decrease in volume four

days after induction of Kdm2b silencing, moreover, half of the xenografts bearing shKDM2B-A and one out of eight xenografts bearing shKDM2B-C completely regressed 10 days post-induction (Fig 3A and B). At the endpoint, tumor xenografts with silenced Kdm2b were significantly smaller compared with the xenografts overexpressing the scramble RNA control (Fig. 3C). We also xenografted JuB2 cells expressing the silencing vector for Kdm1a or Kdm2a. Although tumor volume repression was initially observed post-doxycycline treatment, tumor regrowth was observed 10 post-doxycycline treatment signifying that other histone demethylases or proteins can rescue Kdm1a or Kdm2a function *in vivo* or some cell populations were not affected by their knockdown (Fig. 3A).

These results suggest that Kdm2b is important for HSA cell survival both *in vitro* and *in vivo* and its local catalytic activity is responsible for the phenotype.

KDM2B knockdown induces apoptosis via accumulation of DNA damages

To understand the mechanisms by which Kdm2b regulates HSA cell survival, we performed RNA-seq followed by gene set enrichment analyses (GSEA) in JuB2 cells expressing shKDM2B-A versus JuB2 cells expressing scrRNA-1. Silencing of Kdm2b showed negative correlations with angiogenesis and glycolysis pathways, which might reflect decreased HSA cell viability (Supplementary Fig. 3A). Interestingly, expressions of genes downregulated in

response to ultraviolet (UV) radiation (HALLMARK_UV_RESPONSE_DN) were decreased by Kdm2b knockdown (Fig. 4A). Considering this correlation and the fact that UV response can trigger DNA damage response[20], we speculated that DNA damage might be related to *KDM2B* knockdown phenotypes. This speculation was further supported by positive enrichment of the G2M checkpoint pathway and the interferon response pathway, which has been reported to be associated with mitochondrial and nuclear DNA damage (Supplementary Fig. 3A)[21–24]. These results were validated by qRT-PCR (Fig. 4B, Supplementary Fig. 3B to E). To further dissect the mechanism, we examined the expression levels of proteins involved in DNA repair pathway. Total Atm, c-Fos, and γH2A.X expressions were upregulated in HSA cell lines compared to CnAOEC and their expressions were significantly decreased by *KDM2B* knockdown (Fig 4C and D). Phosphorylated-Atm (pAtm), an active form of Atm, was also decreased by *KDM2B* knockdown. Next, we carried out alkaline comet assay to detect DNA strand breaks in HSA cell lines upon *KDM2B* silencing. Our results showed that *KDM2B* silencing drastically increased tail DNA percentages, tail lengths, and tail momentums compared to the scramble control (Fig. 4E and F). Furthermore, flow cytometry analysis using propidium iodide (PI) revealed that JuB2 with silenced *KDM2B* increased aneuploid peaks although parental HSA cells also showed aneuploidy (Fig 5A and B, Supplementary Fig. 4A and B). In contrast, overexpression of WT Kdm2b in JuB2 HSA cells resulted to significantly decreased aneuploid cell population

compared to empty vector (EV) expressing JuB2 cells (Fig 5C and D). In addition, active apoptosis markers, cleaved-caspase 3, Bax and phosphorylated Erk1/2, were increased in cells with silenced *KDM2B* compared to the scramble control cells (Fig 5E). Furthermore, CnAOEC overexpressing WT Kdm2b continued proliferating beyond day 20 while the EV expressing CnAOEC showed decreased cell proliferation and cell death starting at day 11 (Fig 5F). In addition, Kdm2b overexpression decreased the phosphorylation of Erk1/2 proteins at day 19 post-lentiviral Kdm2b overexpression (Fig. 5G and H) and repressed mRNA expressions of cell cycle checkpoint genes such as $p15^{ink4b}$, $p16^{ink4a}$, and *ATR* (Fig. 5I). These results suggest that *KDM2B* knockdown in HSA cells induces cell death via apoptosis caused by accumulation of DNA damages due to low expression of proteins involved in DNA repair.

Kdm2b is highly expressed in clinical cases of HSA

We demonstrated that Kdm2b upregulation was important for HSA cell survival, but Kdm2b expression in clinical HSA cases has not been investigated. To this end, we analyzed seventeen clinical cases of HSA and compared the immunohistochemical Kdm2b expression between HSA cells and normal endothelial cells in the same sample. Our results showed that Kdm2b was highly expressed in HSA cells compared to normal endothelial cells in almost all the cases examined regardless of proliferation patterns or degree of differentiation (Fig 6A and

B). The average Kdm2b score in HSA cells was significantly higher than that in normal endothelial cells (Fig. 6C). We then also examined the benign endothelial tumor, hemangioma (HMA), for Kdm2b expression. Interestingly, Kdm2b expression levels in hemangioma cells were likely lower than normal endothelial cells in the same sample (Fig. 6D to F, p=0.096). The average Kdm2b expression scores in HSA were significantly higher than in HMA cells when the average Kdm2b scores in tumor cells were normalized to normal endothelial cells in the same slides (Fig. 6G). Kdm2b expressions were also analyzed in histologically-similar tumors, hemangiopericytoma (HPC), melanoma, and fibrosarcoma cells. Results showed that HPC, melanoma, and fibrosarcoma cells had similar Kdm2b expression compared to normal endothelial cells in the same slide (Supplementary Fig. 5A to C). These results suggest that Kdm2b expresses in clinical HSA samples and can be used as a biomarker to differentiate HSA and HMA. In addition, Kdm2b may also be used as a molecular marker to differentiate HSA from HPC, melanoma, and fibrosarcoma.

GSK-J4 inhibits HSA cell viability

We demonstrated that KDM2B inhibition through shRNA could induce HSA cell death. Based on this, we hypothesized that pharmacological Kdm2b inhibition could also induce HSA cell death. To test this hypothesis, we treated HSA cell lines with different concentrations of

GSK-J4 and compared it to doxorubicin-treated cells. GSK-J4 inhibited HSA cell viability at a lower concentration in JuB2, JuB4, and Ud6 cell lines compared to doxorubicin (Fig. 7A). HSA cell lines treated with GSK-J4 have higher expressions of cleaved-caspase 3 compared to HSA cells treated with doxorubicin. In contrast, GSK-J4 treated HSA cells have decreased t-Atm and γH2A.X expression compared to HSA cells treated with DMSO control (Fig.7B).

To determine whether GSK-J4 can be used as an alternative drug for HSA treatment, we treated nude mice harboring JuB2 tumors with DMSO, GSK-J4 or doxorubicin. GSK-J4 treatment significantly decreased the tumor growth over time and tumor weights at the endpoint compared to DMSO treatment (Fig 7C-E). Although Doxorubicin treatment also led to decreased tumor growth, it had significant toxicity and led to 83% mortality in 21 days (Fig. 7F). In contrast, GSK-J4 did not induce any death during the treatment period. Body and liver weights decreased in doxorubicin-treated mice compared to DMSO or GSK-J4 treated mice (Fig. 7G, Supplementary Fig. 6A). In addition, increased hematopoiesis in bone marrow, a sign of myelosuppression, and dilation of intestines were only observed in mice treated with doxorubicin (Supplementary Fig. 6B and C). These results suggest that GSK-J4 can selectively inhibit HSA cell growth by inducing HSA cell apoptosis without any obvious side-effects. Thus, GSK-J4 could be used as a therapeutic alternative to doxorubicin for HSA treatment.

Discussion

To our knowledge this is the first study which evaluated the role of epigenetic regulators in HSA. We demonstrated that Kdm2b upregulation in HSA cell lines and clinical samples is important for HSA cell survival by regulating DNA damage repair and apoptosis. There are three possible reasons for the high expression of Kdm2b in HSA. Firstly, *KDM2B* upstream regulators may be dysregulated. In bladder cancer, the upregulation of fibroblast growth factor-2 upregulated the KDM2B/EZH2-miR-101 pathway and promoted tumor cell proliferation, survival, and migration[25]. In squamous cell and cervical carcinomas, increased copy number of *MYC* resulted to increased KDM2B expression[26]. Secondly, the *KDM2B* gene itself may have acquired increased copy numbers. We demonstrated that parental HSA cell lines contain an aneuploid cell population. Since cell aneuploidy can cause genomic instability as a result of decreased DNA damage repair activity[27], some genes including *KDM2B* in HSA might have increased copy numbers. Lastly, *KDM2B* might be upregulated to compensate for DNA damage and to integrate genetic stability in HSA genomes. As we mentioned above, flow cytometry analysis revealed multiple aneuploid peaks in HSA cell lines. Aneuploidy has also been reported in clinical cases of HSA and in HSA cell lines, which implies that HSA cells are subject to high level cellular stress[28–30]. In such conditions, HSA cells may bypass cell death caused by accumulated cellular stresses through modulation of gene expression. We showed that

knockdown of Kdm2b in HSA cell lines decreased DNA repair protein expressions and increased DNA damage. In contrast, exogenous expression of Kdm2b in JuB2 and in CnAOEC increased euploid population and inhibited apoptosis, respectively. Kdm2b may ease cellular stress caused by DNA damage in endothelial cells by regulating the DNA repair system.

KDM2B and other histone demethylases are known to have a double-edged function in cancer[8,31]. A study showed that KDM2B suppresses tumorigenesis in gastric cancer by enhancing c-Fos degradation, and that impairment of KDM2B through patient-derived mutations enhances tumor cell proliferation[32]. In contrast, several studies showed that degradation of c-FOS by KDM2B in prostate cancer and glioblastoma multiforme can increase cancer cell resistance to chemotherapy[33,34]. In HSA, we showed that positive regulation of these genes by Kdm2b can enhance HSA cellular viability in contrast to a previous report where KDM2B was shown to promote colon cancer cell survival by negatively regulating DNA damage response-related genes such as ATM and ATR[35]. These contrasting evidences support the role of KDM2B in DNA damage response and suggest that the role of KDM2B in DNA damage response in cancer cells is highly context dependent.

We have presented various evidences which demonstrate the role of Kdm2b as an oncogene in HSA by regulating DNA repair system and apoptosis, and that Kdm2b can be used as a biomarker to aid HSA diagnosis. We also demonstrated that a histone demethylase inhibitor

GSK-J4 can work as a new therapeutic alternative to doxorubicin treatment in HSA. These findings shed light on the epigenetic pathology and provides a new insight for a novel therapy in HSA.

Materials and Methods

Cell culture

The HSA cell lines were donated by Dr. Sakai (Gifu University)[36] and cultured as described previously[37]. CnAOEC was purchased from Cell Applications (CA, USA), and ISO-HAS-B was received from Cell Resource Center for Biomedical Research Cell Bank in Tohoku University (Sendai, Japan)[38]. Both CnAOEC and ISO-HAS-B were cultured in Endothelial Cell Growth Medium 2 Kit (Takara Bio, Inc. Kusatsu, Japan). All cells used were routinely tested for *Mycoplasma* using PCR and were submitted to ICLAS Monitoring Center (Kawasaki, Japan) for Mouse hepatitis virus testing[39,40].

Mice

All mouse experiments were performed under the AAALAC guidelines in Yale University (protocol number: 2018-11286) and Hokkaido University (protocol number:19-0130). Seven-week old female Balb/c Nude mice purchased from Charles River Laboratories (MA,

276 USA) were used for *KDM2B* knockdown experiments. Six-week-old KSN/Slc mice purchased
277 from Japan SLC, Inc. (Shizuoka, Japan) were used for drug treatment experiments. Mice were
278 kept in a temperature-controlled specific-pathogen-free facility on a 12 hr light/dark cycle.
279 Animals in all experimental groups were examined at least twice weekly for tumorigenesis.
280
281 **Tumor xenograft studies**
282 A day before tumor inoculation, KSN/Slc mice were treated with 100 μL of 2.5
283 mg/mL anti-asialo GM1 (Fujifilm Wako Pure Chemical Industries, Osaka, Japan) to increase the
284 success rate of transplantation by depleting NK cells[41]. JuB2 parental HSA cells and JuB2 cells
285 expressing the shRNAs or the scramble shRNA for *KDM2B* in the presence of doxycycline
286 were cultured in 15 cm dishes without doxycycline. Mice were randomly assigned in each group.
287 Three million HSA cells were resuspended in Corning® Matrigel® Basement Membrane Matrix
288 (Corning Inc. NY, USA) and inoculated subcutaneously in mice anesthetized with 3% isoflurane
289 or 100 mg/kg Ketamine and 10 mg/kg Xylazine. Tumor sizes were measured twice weekly one
290 week after inoculation. When the largest tumor reached 150 mm^3 in volume, mice were fed
291 doxycycline-containing food to induce shRNA expression, or treated thrice weekly for three
292 weeks with 50 mg/kg DMSO, 50 mg/kg GSK-J4 (Medchemexpress, NJ, USA), or 5 mg/kg
293 doxorubicin (Fujifilm Wako Pure Chemical Industries) intraperitoneally. Mice were euthanized

with CO_2 when tumors reached 500 mm^3 in volume or when mice exhibited abnormal behavior. Tumors and major organs were weighed and fixed in 10% neutral buffered formalin for histological examination.

Western Blotting

SDS lysis buffer (2% SDS, 50 mM Tris-HCl (pH6.8), 1mM EDTA (pH 8.0)) with EDTA-free proteinase inhibitor cocktail (Sigma-Aldrich, MO, USA) was added in cultured cells. Cell lysates were then sonicated using BRANSON Sonifier 450 (Branson Ultrasonics Corporation, CT, USA) for two secs. Protein concentrations were measured with the Pierce™ BCA Protein Assay Kit (Thermo Fisher Scientific) before adding 4X Sample loading buffer (200 mM Tris-HCl buffer (pH 6.8), 8% SDS, 40% Glycerol, 1% bromophenol blue, 20% 2-mercaptoethanol) and denaturing at 98°C for 10 mins. 3 µg proteins were separated by SDS-PAGE and electrotransferred onto Immobilon®-P transfer membranes (Merck Millipore, MA, USA), blocked with 5% skim milk in Tris-buffered saline with 5% Tween 20 (TBST), or 5% BSA in TBST for one hour at room temperature (RT) and incubated with primary antibody in Can Get Signal Solution® 1 (TOYOBO, Osaka, Japan) overnight at 4°C. The membranes were washed with TBST three times before incubating with the corresponding secondary anti-mouse or anti-rabbit IgG antibody (GE Healthcare) in Can Get Signal Solution® 2

(TOYOBO). Signals were developed with Immobilon® Western Chemiluminescent HRP substrate (Merck Millipore) and visualized in ImageQuant LAS 4000 mini luminescent image analyzer (GE Healthcare). Captured data were processed using ImageJ software[42]. The list of antibodies used in this study can be found as Supplementary Table 1.

Quantitative RT-PCR (qRT-PCR)

Total RNA was extracted with Nucleospin® RNA isolation kit (Macherey-Nagel GmbH & Co. Düren, Germany) following the manufacturer's instructions. Synthesis of cDNA was performed using the PrimeScript™ Reverse Transcriptase (Takara Bio, Inc.) according to the manufacturer's instructions. qRT-PCR was performed with StepOne™ Real Time System (Thermo Fisher Scientific). The oligos for qRT-PCR were designed as described elsewhere[37,43], and listed within Supplementary Table 2.

RNA-sequencing

CnAOEC or JuB2 HSA cells were cultured in 10 cm dishes in triplicate. Upon reaching 80% confluency, RNA was extracted with Nucleospin® RNA isolation kit (Macherey-Nagel GmbH & Co.) following the manufacturer's instructions. RNA samples were submitted to Annoroad (Beijing, China) for further analyses. Quality testing was carried by

measuring RNA integrity (RIN), $OD_{260/280}$ and $OD_{260/230}$. All samples had an RIN of 9.3 or better and OD readings were within the range of 1.8-2.2. RNA-seq libraries were constructed using NEBNext® Ultra RNA Library Prep Kit for llumina® (New England Biolabs, MA, USA) and sequenced with the Illumina HiSeq X-Ten platform (Illumina, CA, USA) to generate a minimum of 20 million paired-end 150 bp reads. Sequencing reads were mapped to the canine reference genome CanFam3.1 using STAR and aligned using RSEM[44,45]. Differential expression analyses were carried out using edgeR[46], and gene expression profiles were analyzed by GSEA v4.03[47,48]. The gene set database of h. all. v7.1. symbols. gmt (Hallmarks) was used.

shRNA vector construction

The shRNAs used in this study were designed using the Hannon lab shRNA design tool (http://hannonlab.cshl.edu/GH_shRNA.html, Cold Spring Harbor Laboratory). Oligos were inserted to pLKO.1-TRC or pInducer10-mir-RUP-PheS vector, a gift from David Root (Addgene plasmid # 10878; http://n2t.net/addgene:10878; RRID:Addgene_10878)[49] and from Stephen Elledge (Addgene plasmid # 44011; http://n2t.net/addgene:44011; RRID:Addgene 44011)[50], respectively. shRNA expressions were induced by supplementing 2 μM doxycycline in the culture medium. The list of oligonucleotide sequences used for shRNA knockdown can be found as Supplementary Table 3.

348

349 **Overexpression vector construction**

350 The coding sequence of canine *KDM2B* (ENSCAFT00000093772.1) was cloned from
351 cDNA synthesized from canine heart. Mutant Kdm2b (H283Y, C586A, ΔPHD) were
352 synthesized as described elsewhere[15,51]. The amplicon tagged with FLAG sequences at its 3' end
353 was ligated into CSII-CMV-MCS-IRES2-Bsd vector, a gift from Dr. Miyoshi (RIKEN
354 BioResource Center, Ibaraki, Japan), with In-Fusion® HD Cloning Kit (Takara Bio, Inc.)
355 according to the manufacturer's instruction. The list of oligonucleotide sequences used for CDS
356 cloning are can be found as Supplementary Table 4.

357

358 **Lentivirus production**

359 Lentiviruses were produced following a protocol described elsewhere with a slight
360 modification that virus containing culture medium was used without concentration[37]. Selection
361 of positive clones were done by culturing of cells in 10 μg/ml blasticidin- or 4 μg/ml
362 puromycin-containing cell medium.

363

364 **Alkaline comet assay**

365 JuB2 overexpressing shRNA for *KDM2B* or scrRNA were cultured in

366 doxycycline-containing medium for four days. $4X10^4$ cells were used for alkaline comet assay
367 as described previously. 20 μg/mL PI was used for staining and the comets were visualized with
368 BZ-9000 (BIOREVO) fluorescence microscope (Keyence, Osaka, Japan). Experiments were
369 performed at least three times with triplicates.
370
371 **Cell cycle analysis**
372 When HSA cells reach 70% confluency, they were stained with 1 μL of 0.1M BrdU for
373 45 mins at 37°C. Cells were washed with phosphate-buffered saline (PBS) and trypsinized
374 routinely. The cells were fixed in 70% ethanol overnight and washed with 0.5% Triton X-100 in
375 PBS (PBST) before resuspending the cells in 500 μL of 2N HCl-0.5% Triton X-100 for 30 mins
376 at RT and neutralizing with 500 μL of 0.1M $Na_2B_4O_7 \cdot 10H_2O$ (pH 8.5) for 30 mins at RT. After
377 blocking with 1% BSA-0.3% Triton X-100 in PBS for 1 hr and washing with PBST, cells were
378 counted and divided into two tubes; $2.5X10^5$ cells were used as controls and incubated in the
379 blocking buffer while $6X10^5$ cells were incubated with anti-BrdU monoclonal antibody (1:100;
380 MOBU-1 clone, B35128, Thermo Fisher Scientific) for 1 hr at RT. Excess primary antibodies
381 were washed before staining with AlexaFluor 488 (1:1000; Thermo Fisher Scientific). DNA was
382 stained with 10 μg/200 μL Propidum Iodide (Dojindo Molecular Technologies, Inc., Kumamoto,
383 Japan). Cell cycle and cell proliferation were analyzed in BD FACSVerse™ flow cytometer (BD

384 Biosciences, NJ, USA). Results were analyzed with FCS Express 4 software (De Novo
385 Software, CA, USA). Experiments were performed at least three times with triplicates.
386
387 **Cell viability analysis**
388 Cell viability was measured with Cell Counting Kit-8 (Dojindo Molecular
389 Technologies, Inc.) according to the manufacturer's instructions. The absorbance at 450 nm was
390 measured with NanoDrop™ 2000 (Thermo Fisher Scientific). Determination of IC_{50} were
391 performed using Ky Plot 6.0 software (KyensLab, Inc., Tokyo, Japan) as described elsewhere[52].
392 Experiments were performed at least three times with triplicates.
393
394 **Colony formation assay**
395 500 HSA cells were seeded in 6-well culture plates containing 2 mL normal medium
396 supplemented with DMSO or 2 μM doxycycline. Cells were cultured until the largest colony
397 reached 2 mm in diameter. Cells were fixed with 4% paraformaldehyde for 20 mins at RT,
398 stained with 0.01% Crystal Violet (Sigma-Aldrich, MO, USA) for 30 mins at RT, and the
399 images were captured with ChemiDoc XRS Plus (Bio-rad, CA, USA). Colony areas were
400 measured using ColonyArea plugin for ImageJ[42,53]. Experiments were performed at least three
401 times with triplicates.

Histopathology and immunohistochemistry (IHC)

Written informed consents were obtained from the owners of the patient dogs, and the samples were used only for research purposes. Hematoxylin and eosin staining was performed as described previously[54]. For IHC, tissue sections were deparaffinized, and heat-induced antigen retrieval was performed in citric acid buffer (pH 6.8) with a pressure cooker. Endogenous peroxidases were quenched with 0.3% H_2O_2 in methanol for 15 min at RT before blocking the tissue sections with 10% normal rabbit serum (Nichirei biosciences, Tokyo, Japan) for an hour at RT and incubating with KDM2B antibody (sc-293279, 1:50, Santa Cruz Biotechnology, CA, USA) overnight at 4°C. Slides were washed with 0.01M PBS before incubating with rabbit anti-mouse antibody (Nichirei biosciences) for 30 min at RT. Signals were developed with 3,3'-diaminobenzidine tetrahydrochloride (DAB; Dojindo).

Quantification of IHC scores

Histological slides were scanned with Nano Zoomer 2.0-RS (Hamamatsu Photonics, Hamamatsu, Japan) and processed in QuPath ver 0.2.1[55]. Scanned slides were opened as Brightfield (H-DAB) in QuPath, and staining colors were automatically adjusted using Estimate Stain Vectors function. Healthy tumor regions or normal blood vessels were randomly selected,

and cells were detected using Cell Detection function. Cells were annotated based on their morphologies and location to allow QuPath to automatically classify each cell type correctly using the Create Detection Classifiers function. The measured data was exported and used for further analysis. We used Nuclear: DAB OD max scores for quantitative analysis because Kdm2b signals were found only in heterochromatin regions in nuclei but they had abundant euchromatin region. Furthermore, nonspecific signals from fibrin and erythrocytes were often misinterpreted as nuclear or cytoplasmic signals especially in normal endothelial cells, thus, to make the analysis as precise as possible, we decided to use max intensities in the nuclei.

Statistical analysis

Statistical analyses were performed with Microsoft Excel and R software (version 3.6.3). Student's *t*-tests was used to analyze difference between two groups while the Tukey's test was used to analyze differences between multiple groups. The significance of the differences in tumor volumes of DMSO, GSK-J4 or doxorubicin-treated mice were compared using Dunnet's test while their survival post-treatment were compared using Log-rank test. *p*-values less than 0.05 were considered statistically significant.

Acknowledgements

We are grateful to Dr. Osamu Ichii, Dr. Junpei Yamazaki, and Dr. Noboru Sasaki for their invaluable support during the conduct of the study. We appreciate useful discussions with the members of the Laboratory of Comparative Pathology, Faculty of Veterinary Medicine, Hokkaido University, and the members of Yan laboratory, Department of Pathology, Yale School of Medicine. This research was supported by the Sasagawa Scientific Research Grant for Young Researchers (KG, Research No. 2019-4111) provided by the Japan Science Society and the KAKENHI Grant-in-Aid for Young Scientist (KA, Number 18K14575 and 20K15654) provided by Japan Society for the Promotion of Science.

Availability of data and materials

The RNA sequence data will be deposited in NCBI's Gene Expression Omnibus. All other data supporting the findings of this study can be found within the supplementary files.

Competing interests

The authors declare no competing interests.

Author contributions

KG and KA designed the experiments. KG performed in vitro experiments. KG and KA

456 performed in vivo experiments. YS and HY assisted with the comet assay. KA analyzed the

457 RNA-sequencing data and performed other bioinformatics analyses. KG and KA were

458 responsible for the statistical analyses. QY, AK and TK supervised the experiments. KG and KA

459 wrote the paper.

References

1 Kim J-H, Graef AJ, Dickerson EB, Modiano JF. Pathobiology of Hemangiosarcoma in Dogs: Research Advances and Future Perspectives. *Vet Sci* 2015; **2**: 388–405.

2 Megquier K, Turner-Maier J, Swofford R, Kim J-H, Sarver AL, Wang C *et al.* Comparative Genomics Reveals Shared Mutational Landscape in Canine Hemangiosarcoma and Human Angiosarcoma. *Mol Cancer Res* 2019; **17**: 2410–2421.

3 Sharma S, Kelly TK, Jones PA. Epigenetics in cancer. *Carcinogenesis* 2010; **31**: 27–36.

4 Moosavi A, Motevalizadeh Ardekani A. Role of Epigenetics in Biology and Human Diseases. *Iran Biomed J* 2016; **20**: 246–258.

5 Hong X, Xu Y, Qiu X, Zhu Y, Feng X, Ding Z *et al.* MiR-448 promotes glycolytic metabolism of gastric cancer by downregulating KDM2B. *Oncotarget* 2016; **7**: 22092–22102.

6 He J, Nguyen AT, Zhang Y. KDM2b/JHDM1b, an H3K36me2-specific demethylase, is required for initiation and maintenance of acute myeloid leukemia. *Blood* 2011; **117**: 3869–3880.

7 Kottakis F, Foltopoulou P, Sanidas I, Keller P, Wronski A, Dake BT *et al.* NDY1/KDM2B functions as a master regulator of polycomb complexes and controls self-renewal of breast cancer stem cells. *Cancer Res* 2014; **74**: 3935–3946.

8 Yan M, Yang X, Wang H, Shao Q. The critical role of histone lysine demethylase KDM2B in cancer. *Am J Transl Res* 2018; **10**: 2222–2233.

9 Sorenmo KU, Baez JL, Clifford CA, Mauldin E, Overley B, Skorupski K *et al.* Efficacy and Toxicity of a Dose-Intensified Doxorubicin Protocol in Canine Hemangiosarcoma. *J Vet Intern Med* 2004; **18**: 209–213.

10 Clifford CA, Mackin AJ, Henry CJ. Treatment of Canine Hemangiosarcoma: 2000 and Beyond. *J Vet Intern Med* 2000; **14**: 479–485.

11 Brown NO, Patnaik AK, MacEwen EG. Canine hemangiosarcoma: retrospective analysis of 104 cases. *J Am Vet Med Assoc* 1985; **186**: 56–58.

12 Batschinski K, Nobre A, Vargas-Mendez E, Tedardi MV, Cirillo J, Cestari G *et al.* Canine visceral hemangiosarcoma treated with surgery alone or surgery and doxorubicin: 37 cases (2005-2014). *Can Vet J Rev Veterinaire Can* 2018; **59**: 967–972.

13 Carvalho C, Santos R, Cardoso S, Correia S, Oliveira P, Santos M *et al.* Doxorubicin: The Good, the Bad and the Ugly Effect. *Curr Med Chem* 2009; **16**: 3267–3285.

14 Odom AL, Hatwig CA, Stanley JS, Benson AM. Biochemical determinants of adriamycin® toxicity in mouse liver, heart and intestine. *Biochem Pharmacol* 1992; **43**: 831–836.

15 Li Y, Zhang M, Sheng M, Zhang P, Chen Z, Xing W *et al.* Therapeutic potential of GSK-J4, a histone demethylase KDM6B/JMJD3 inhibitor, for acute myeloid leukemia. *J Cancer Res Clin Oncol* 2018; **144**: 1065–1077.

16 Heinemann B, Nielsen JM, Hudlebusch HR, Lees MJ, Larsen DV, Boesen T *et al.* Inhibition of demethylases by GSK-J1/J4. *Nature* 2014; **514**: E1–E2.

17 Wang T, Chen K, Zeng X, Yang J, Wu Y, Shi X *et al.* The Histone Demethylases Jhdm1a/1b Enhance Somatic Cell Reprogramming in a Vitamin-C-Dependent Manner. *Cell Stem Cell* 2011; **9**: 575–587.

18 Tzatsos A, Pfau R, Kampranis SC, Tsichlis PN. Ndy1/KDM2B immortalizes mouse embryonic fibroblasts by repressing the Ink4a/Arf locus. *Proc Natl Acad Sci* 2009; **106**: 2641–2646.

19 Zhou Q, Zhang Y, Wang B, Zhou W, Bi Y, Huai W *et al.* KDM2B promotes IL-6 production and inflammatory responses through Brg1-mediated chromatin remodeling. *Cell Mol Immunol* 2020; **17**: 834–842.

20 Stokes MP, Rush J, Macneill J, Ren JM, Sprott K, Nardone J *et al.* Profiling of UV-induced ATM/ATR signaling pathways. *Proc Natl Acad Sci U S A* 2007; **104**: 19855–19860.

21 Brzostek-Racine S, Gordon C, Scoy SV, Reich NC. The DNA Damage Response Induces IFN. *J Immunol* 2011; **187**: 5336–5345.

22 Mboko WP, Mounce BC, Wood BM, Kulinski JM, Corbett JA, Tarakanova VL. Coordinate Regulation of DNA Damage and Type I Interferon Responses Imposes

an Antiviral State That Attenuates Mouse Gammaherpesvirus Type 68 Replication in Primary Macrophages. *J Virol* 2012; **86**: 6899–6912.

23 Chen J, Harding SM, Natesan R, Tian L, Benci JL, Li W *et al.* Cell Cycle Checkpoints Cooperate to Suppress DNA- and RNA-Associated Molecular Pattern Recognition and Anti-Tumor Immune Responses. *Cell Rep* 2020; **32**. doi:10.1016/j.celrep.2020.108080.

24 Tigano M, Vargas DC, Fu Y, Tremblay-Belzile S, Sfeir A. Nuclear sensing of mitochondrial DNA breaks enhances immune surveillance. *bioRxiv* 2020; : 2020.01.31.929075.

25 Kottakis F, Polytarchou C, Foltopoulou P, Sanidas I, Kampranis SC, Tsichlis PN. FGF-2 regulates cell proliferation, migration, and angiogenesis through an NDY1/KDM2B-miR-101-EZH2 pathway. *Mol Cell* 2011; **43**: 285–298.

26 Peta E, Sinigaglia A, Masi G, Di Camillo B, Grassi A, Trevisan M *et al.* HPV16 E6 and E7 upregulate the histone lysine demethylase KDM2B through the c-MYC/miR-146a-5p axys. *Oncogene* 2018; **37**: 1654–1668.

27 Sheltzer JM, Blank HM, Pfau SJ, Tange Y, George BM, Humpton TJ *et al.* Aneuploidy Drives Genomic Instability in Yeast. *Science* 2011; **333**: 1026–1030.

28 Fosmire SP, Dickerson EB, Scott AM, Bianco SR, Pettengill MJ, Meylemans H *et al.* Canine malignant hemangiosarcoma as a model of primitive angiogenic endothelium. *Lab Invest* 2004; **84**: 562–572.

29 Thomas R, Borst L, Rotroff D, Motsinger-Reif A, Lindblad-Toh K, Modiano JF *et al.* Genomic profiling reveals extensive heterogeneity in somatic DNA copy number aberrations of canine hemangiosarcoma. *Chromosome Res Int J Mol Supramol Evol Asp Chromosome Biol* 2014; **22**: 305–319.

30 Zhu J, Tsai H-J, Gordon MR, Li R. Cellular Stress Associated with Aneuploidy. *Dev Cell* 2018; **44**: 420–431.

31 Kozub MM, Carr RM, Lomberk GL, Fernandez-Zapico ME. LSD1, a double-edged sword, confers dynamic chromatin regulation but commonly promotes aberrant cell growth. *F1000Research* 2017; **6**: 2016.

32 Han X-R, Zha Z, Yuan H-X, Feng X, Xia Y-K, Lei Q-Y *et al.* KDM2B/FBXL10 targets

549 c-Fos for ubiquitylation and degradation in response to mitogenic stimulation.
550 *Oncogene* 2016; **35**: 4179–4190.

551 33 Kurt IC, Sur I, Kaya E, Cingoz A, Kazancioglu S, Kahya Z *et al.* KDM2B, an
552 H3K36-specific demethylase, regulates apoptotic response of GBM cells to TRAIL.
553 *Cell Death Dis* 2017; **8**: e2897.

554 34 Ge R, Wang Z, Zeng Q, Xu X, Olumi AF. F-box protein 10, an NF-κB-dependent
555 anti-apoptotic protein, regulates TRAIL-induced apoptosis through modulating
556 c-Fos/c-FLIP pathway. *Cell Death Differ* 2011; **18**: 1184–1195.

557 35 Chen L, Fu L, Kong X, Xu J, Wang Z, Ma X *et al.* Jumonji domain-containing
558 protein 2B silencing induces DNA damage response via STAT3 pathway in
559 colorectal cancer. *Br J Cancer* 2014; **110**: 1014–1026.

560 36 Murai A, Asa SA, Kodama A, Hirata A, Yanai T, Sakai H. Constitutive
561 phosphorylation of the mTORC2/Akt/4E-BP1 pathway in newly derived canine
562 hemangiosarcoma cell lines. *BMC Vet Res* 2012; **8**: 128.

563 37 Aoshima K, Fukui Y, Gulay KCM, Erdemsurakh O, Morita A, Kobayashi A *et al.*
564 Notch2 signal is required for the maintenance of canine hemangiosarcoma cancer
565 stem cell-like cells. *BMC Vet Res* 2018; **14**: 301.

566 38 Masuzawa M, Fujimura T, Hamada Y, Fujita Y, Hara H, Nishiyama S *et al.*
567 Establishment of a human hemangiosarcoma cell line (ISO-HAS). *Int J Cancer*
568 1999; **81**: 305–308.

569 39 Harasawa R, Mizusawa H, Fujii M, Yamamoto J, Mukai H, Uemori T *et al.* Rapid
570 detection and differentiation of the major mycoplasma contaminants in cell cultures
571 using real-time PCR with SYBR Green I and melting curve analysis. *Microbiol*
572 *Immunol* 2005; **49**: 859–863.

573 40 Harasawa R, Mizusawa H, Nozawa K, Nakagawa T, Asada K, Kato I. Detection and
574 tentative identification of dominant mycoplasma species in cell cultures by
575 restriction analysis of the 16S-23S rRNA intergenic spacer regions. *Res Microbiol*
576 1993; **144**: 489–493.

577 41 Yoshino H, Ueda T, Kawahata M, Kobayashi K, Ebihara Y, Manabe A *et al.* Natural
578 killer cell depletion by anti-asialo GM1 antiserum treatment enhances human

579 hematopoietic stem cell engraftment in NOD/Shi- scid mice. *Bone Marrow*
580 *Transplant* 2000; **26**: 1211–1216.

581 42 Schneider CA, Rasband WS, Eliceiri KW. NIH Image to ImageJ: 25 years of image
582 analysis. *Nat Methods* 2012; **9**: 671–675.

583 43 Peters IR, Peeters D, Helps CR, Day MJ. Development and application of multiple
584 internal reference (housekeeper) gene assays for accurate normalisation of canine
585 gene expression studies. *Vet Immunol Immunopathol* 2007; **117**: 55–66.

586 44 Dobin A, Davis CA, Schlesinger F, Drenkow J, Zaleski C, Jha S *et al.* STAR:
587 ultrafast universal RNA-seq aligner. *Bioinformatics* 2013; **29**: 15–21.

588 45 Li B, Dewey CN. RSEM: accurate transcript quantification from RNA-Seq data with
589 or without a reference genome. *BMC Bioinformatics* 2011; **12**: 323.

590 46 Robinson MD, McCarthy DJ, Smyth GK. edgeR: a Bioconductor package for
591 differential expression analysis of digital gene expression data. *Bioinformatics*
592 2010; **26**: 139–140.

593 47 Mootha VK, Lindgren CM, Eriksson K-F, Subramanian A, Sihag S, Lehar J *et al.*
594 PGC-1alpha-responsive genes involved in oxidative phosphorylation are
595 coordinately downregulated in human diabetes. *Nat Genet* 2003; **34**: 267–273.

596 48 Subramanian A, Tamayo P, Mootha VK, Mukherjee S, Ebert BL, Gillette MA *et al.*
597 Gene set enrichment analysis: A knowledge-based approach for interpreting
598 genome-wide expression profiles. *Proc Natl Acad Sci* 2005; **102**: 15545–15550.

599 49 Moffat J, Grueneberg DA, Yang X, Kim SY, Kloepfer AM, Hinkle G *et al.* A
600 Lentiviral RNAi Library for Human and Mouse Genes Applied to an Arrayed Viral
601 High-Content Screen. *Cell* 2006; **124**: 1283–1298.

602 50 Meerbrey KL, Hu G, Kessler JD, Roarty K, Li MZ, Fang JE *et al.* The pINDUCER
603 lentiviral toolkit for inducible RNA interference in vitro and in vivo. *Proc Natl Acad*
604 *Sci U S A* 2011; **108**: 3665–3670.

605 51 Zhou Z, Yang X, He J, Liu J, Wu F, Yu S *et al.* Kdm2b Regulates Somatic
606 Reprogramming through Variant PRC1 Complex-Dependent Function. *Cell Rep*
607 2017; **21**: 2160–2170.

608 52 Morita A, Aoshima K, Gulay KCM, Onishi S, Shibata Y, Yasui H *et al.* High drug
609 efflux pump capacity and low DNA damage response induce doxorubicin resistance
610 in canine hemangiosarcoma cell lines. *Res Vet Sci* 2019; **127**: 1–10.

611 53 Guzmán C, Bagga M, Kaur A, Westermarck J, Abankwa D. ColonyArea: An ImageJ
612 Plugin to Automatically Quantify Colony Formation in Clonogenic Assays. *PLOS*
613 *ONE* 2014; **9**: e92444.

614 54 Maharani A, Aoshima K, Onishi S, Gulay KCM, Kobayashi A, Kimura T. Cellular
615 atypia is negatively correlated with immunohistochemical reactivity of CD31 and
616 vWF expression levels in canine hemangiosarcoma. *J Vet Med Sci* 2018; **80**:
617 213–218.

618 55 Bankhead P, Loughrey MB, Fernández JA, Dombrowski Y, McArt DG, Dunne PD *et*
619 *al.* QuPath: Open source software for digital pathology image analysis. *Sci Rep*
620 2017; **7**: 16878.

621

622 **Figure legends**

623

624 **Fig. 1 Epigenetic regulators are dysregulated in endothelial cell tumors.**

625 **A,** Transcripts per million (TPM) scores of histone demethylases in CnAOEC and JuB2 HSA
626 cell line. **B,** qRT-PCR verification of select histone demethylases in CnAOEC and HSA cell
627 lines. **C,** Western blotting for Kdm1a, Kdm2a, and Kdm2b in CnAOEC and HSA cell lines. **D,**
628 Quantitative analysis of Kdm1a, Kdm2a, and Kdm2b protein expressions in CnAOEC and HSA
629 cell lines. **E,** qRT-PCR analysis of *KDM1A*, *KDM2A*, and *KDM2B* mRNA expressions in
630 HUVEC and ISO-HAS-B. **F,** Western blotting for KDM1A, KDM2A, and KDM2B in HUVEC
631 and ISO-HAS-B. **G,** Quantitative analysis of KDM1A, KDM2A, and KDM2B protein
632 expressions in HUVEC and ISO-HAS-B. Data are presented as mean values ± s.d. *p <0.05
633 **p<0.01 ***p<0.001, Student's t-test; ^{c}p<0.001, Tukey's test.

634

635 **Fig. 2 Kdm2b is important for HSA cell survival *in vitro*.**

636 **A,** Western blotting of Kdm1a, Kdm2a, or Kdm2b to verify the silencing efficiency of shRNA
637 vectors developed for Kdm1a, Kdm2a, and Kdm2b. **B,** Cell viability analysis after the induction
638 of the inducible shRNA vector using doxycycline. **C,** Colony formation assay of JuB2 cells after
639 Kdm1a, Kdm2a, or Kdm2b silencing. **D,** Quantitative analysis of **C**. **E,** Cell viability analysis

after rescue overexpression of WT Kdm2b, or dominant negative mutants for the JmjC (Kdm2b^{H283Y}), CxxC (Kdm2b^{C586A}), or PHD (Kdm2b$^{\Delta PHD}$) domains. Data are presented as mean values ± s.d. ***p<0.001, Two-way ANOVA.

Fig. 3 Kdm2b is important in HSA cell survival *in vivo*.

A, Tumor growth at different time points before and after the induction of the shRNA expression in JuB2 cells inoculated in nude mice. ***p<0.001, two-way ANOVA with Dunnett's post-hoc test for tumor volumes after starting doxycycline treatments (arrow). **B and C,** Tumor sizes and weights of tumors harboring scramble RNA or shRNA for Kdm1a, Kdm2a, or Kdm2b 78 days after tumor transplantation. Scale = 1 cm. **p<0.01 ***p<0.001, Dunnett's test. Data are presented as mean values ± s.d.

Fig. 4 Kdm2b positively regulates DNA repair pathway.

A, GSEA enrichment plot for UV_Response_DN in shKDM2B-A versus scrRNA-1. **B,** qRT-PCR verification of gene expressions listed in UV_Response_DN gene set. **C and D,** Western blotting for Atm, c-Fos, and γH2A.X in normal endothelial cells and HSA cell lines (**C**) and in JuB2 cells expressing shRNA control or shKDM2B (**D**). **E,** Representative images of alkaline comet assays in scrRNA or shKDM2B JuB2 cells. **F,** Tail DNA percentages, lengths,

and momentums of JuB2 HSA cells harboring scrRNA or shRNA for Kdm2b. Data are presented as mean values ± s.d. ***p<0.001, Tukey's test.

Fig. 5 Kdm2b regulates aneuploidy and apoptosis in HSA.

A, Histograms of PI intensities in scrRNA and shKDM2B JuB2 cells. **B,** Percentages of aneuploid cells in shRNA and shKDM2B JuB2 cells. ***p<0.001, Tukey's test. **C,** Histograms of PI intensities in EV infected JuB2 cells and WT Kdm2b JuB2 cells. **D,** Percentages of aneuploid cells in EV JuB2 and WT Kdm2b JuB2. ***p<0.001, Student-t test. **E,** Western blotting for cleaved-caspase 3, Bax and Erk 1/2 in JuB2 HSA cells expressing scrRNA controls or shKDM2B RNAs. **F,** Phase contrast images of CnAOEC cells infected with EV or overexpressing WT Kdm2b at day 1 and day 19. Scale = 100 μm. **G,** Western blotting of Erk 1/2 in CnAOEC infected with EV or overexpressing WT Kdm2b. **H,** Quantification of Kdm2b and phosphorylated Erk 1/2 expression in EV infected or WT Kdm2b expressing CnAOEC normalized with Actin and total Erk 1/2, respectively. **I,** qRT-PCR analysis of cell cycle related genes after overexpression of WT Kdm2B in normal endothelial cells. Data are presented as mean values ± s.d. **p<0.01 ***p<0.001, Student's t-test.

Fig. 6 Kdm2b can be used as a differential biomarker for HSA.

676 **A,** Representative images of hematoxylin-eosin staining (HE) and immunohistochemistry (IHC)
677 for clinical HSA samples. Proliferation patterns are indicated with case numbers. Scale = 100
678 μm. **B,** Max nuclear DAB intensities in individual endothelial cells (EC) and tumor cells
679 (Tumor) of each HSA case. **C,** Average max nuclear DAB intensities of EC and tumor cells in
680 each HSA case. **D,** Representative HE and IHC images of hemangioma (HMA), a benign
681 endothelial cell tumor. Scale = 100 μm. **E,** Max nuclear DAB intensities in individual EC and
682 tumor cells of each HMA case. **F,** Average max nuclear DAB intensities of EC and tumor cells
683 in each HMA case. **G,** Comparison of relative Kdm2b intensity of HSA and HMA cells
684 normalized by normal endothelial cells in their respective slides. Data are presented as mean
685 values ± s.d. $^{**}p<0.01$, Student's *t*-test.
686
687 **Fig. 7 GSK-J4 inhibits HSA cell proliferation *in vitro* and *in vivo*.**
688 **A,** Survival rates and IC_{50} values of GSK-J4 or doxorubicin-treated HSA cell lines. **B,** Western
689 blotting for γH2A.X, Atm and cleaved-caspase 3 in HSA cells treated with GSK-J4 or
690 doxorubicin. **C,** Tumor growth curves of JuB2 HSA cell xenografts in nude mice. Treatment
691 with DMSO, GSK-J4, or doxorubicin started at day 45 (arrow). n indicates the number of mice.
692 $^{**}p < 0.01$, two-way ANOVA with Dunnett's post-hoc test. **D,** Gross images of collected tumors
693 at day 64. n indicates the number of collected tumors. **E,** Tumor weights of DMSO, GSK-J4, or

694 doxorubicin-treated nude mice at necropsy. **F,** Kaplan-Meier survival curves of DMSO, GSK-J4,

695 or doxorubicin-treated nude mice after starting treatments. $^{**}p < 0.01$, Log-rank test. **G,** Body

696 weights of DMSO, GSK-J4, or doxorubicin-treated nude mice at necropsy. Data are presented

697 as mean values ± s.d. $^{**}p<0.01$, Tukey's test.

698

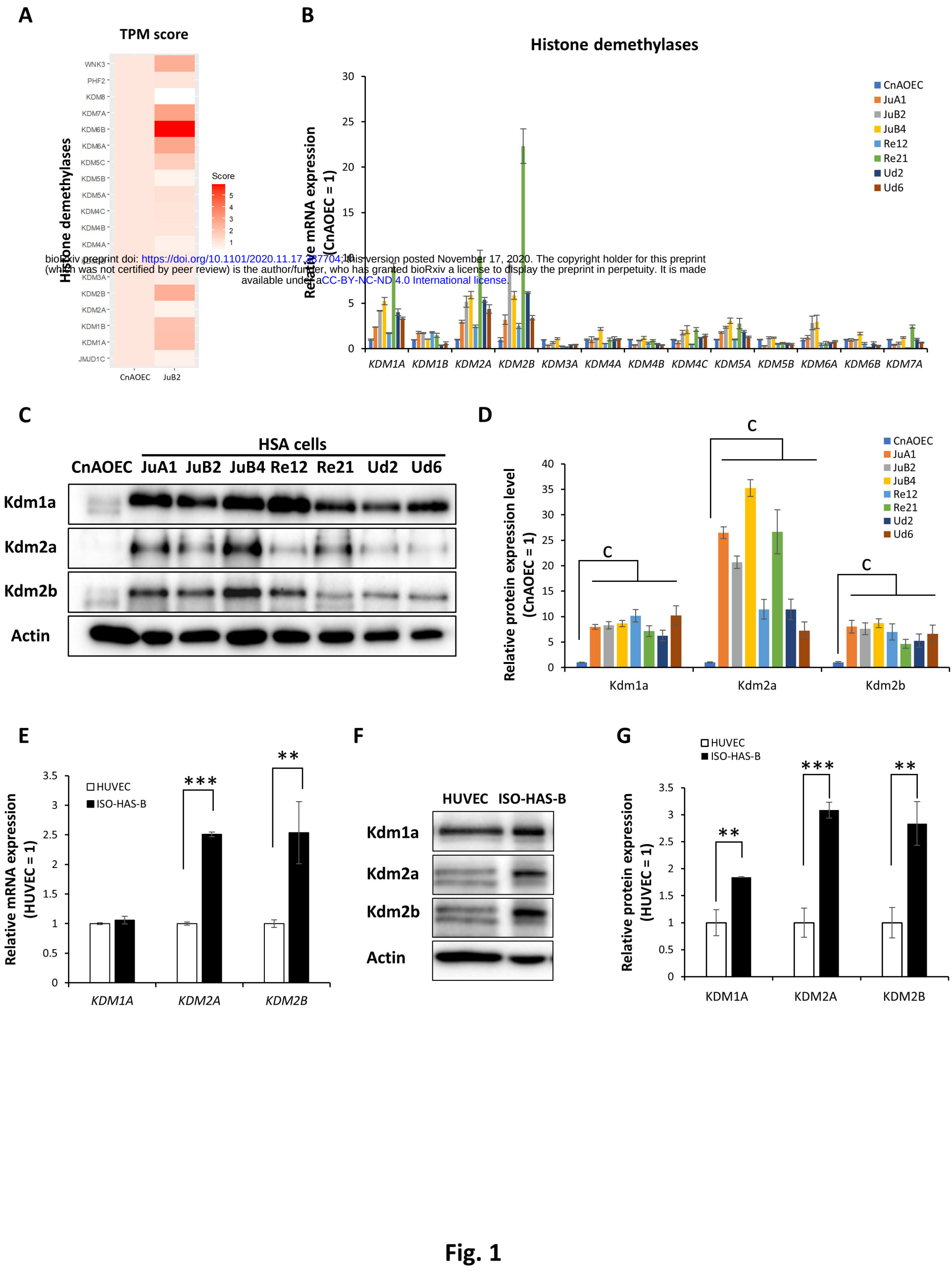

Fig. 1

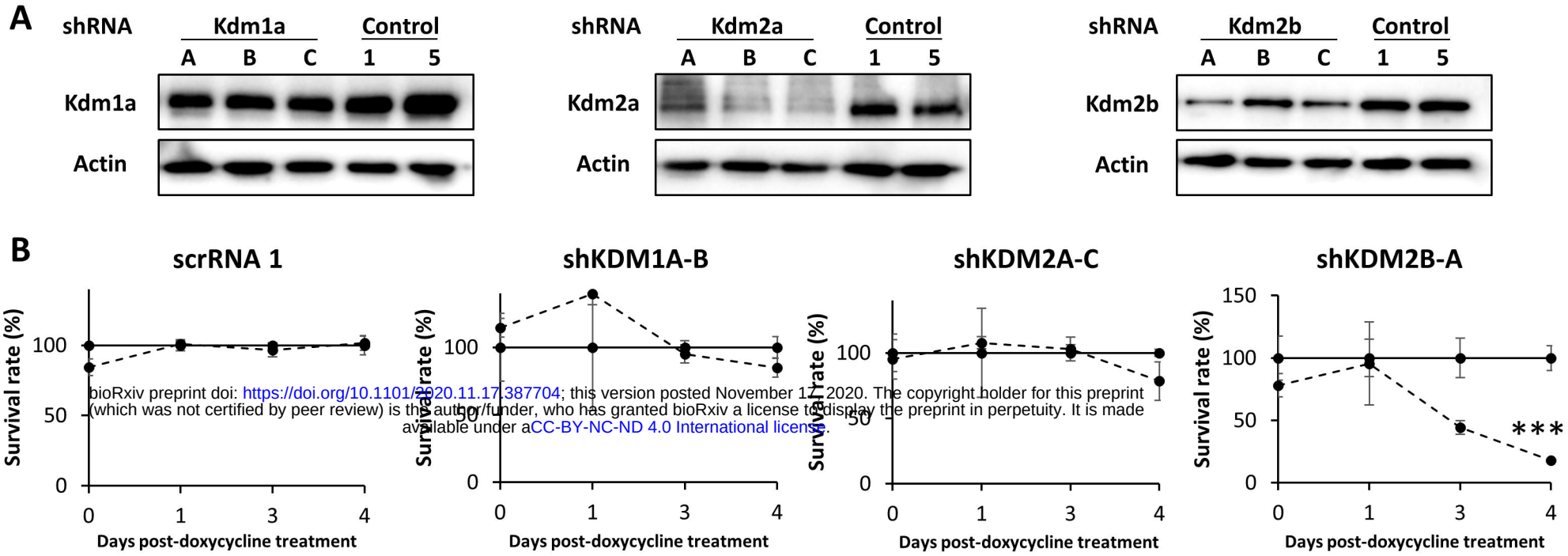

Fig. 2

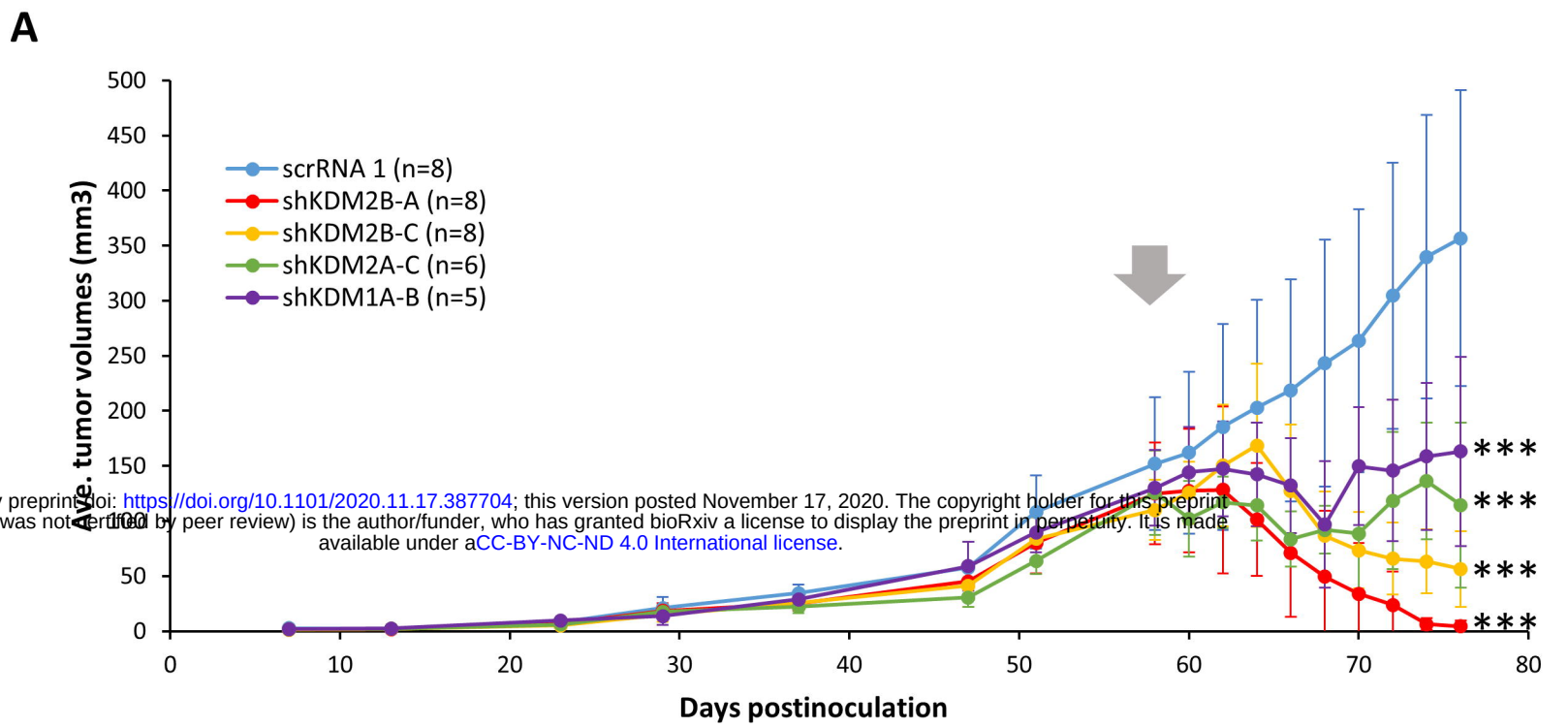

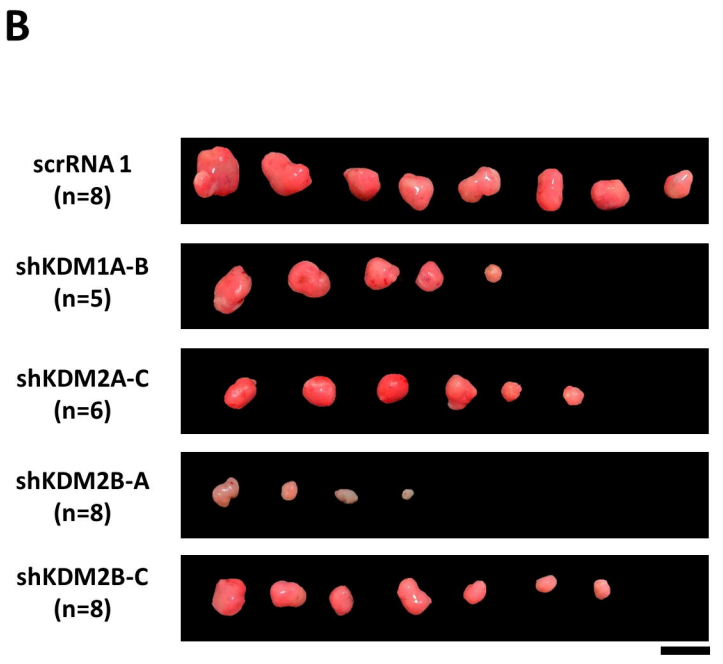

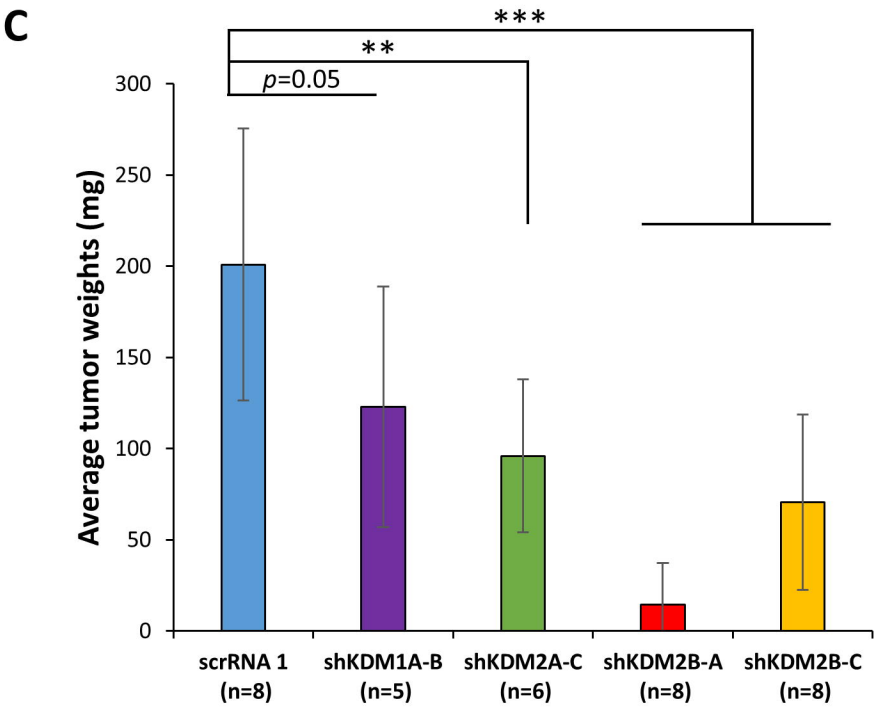

Fig. 3

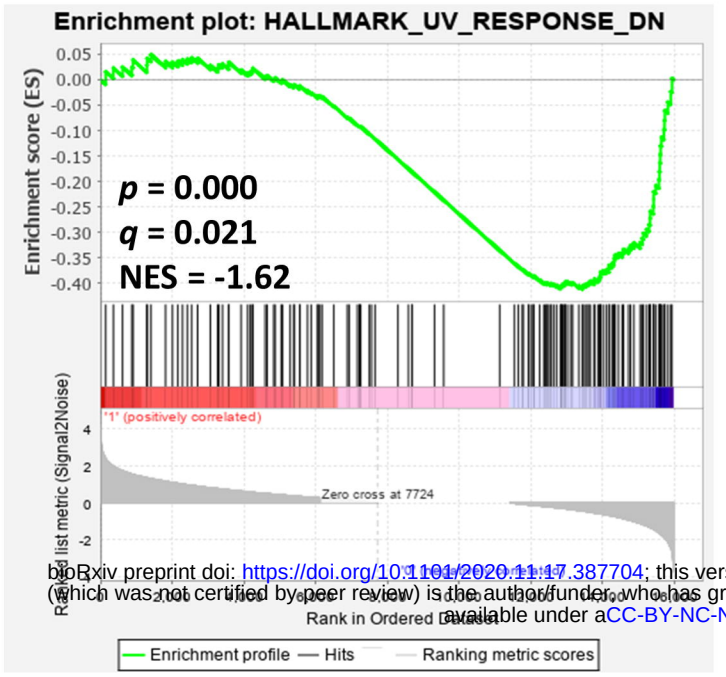

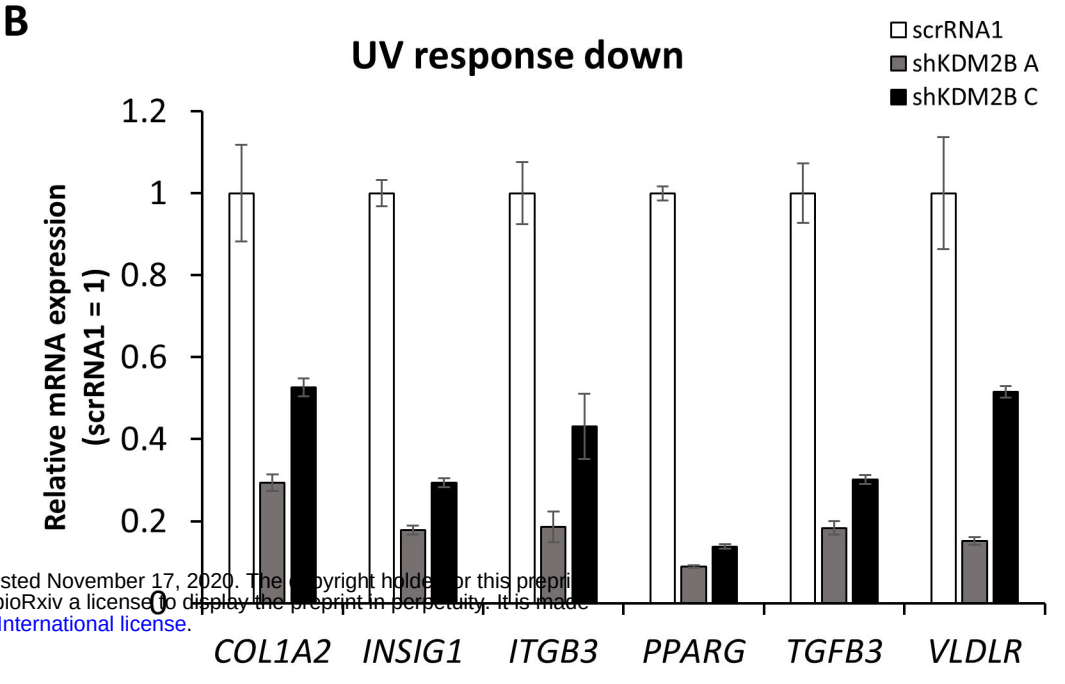

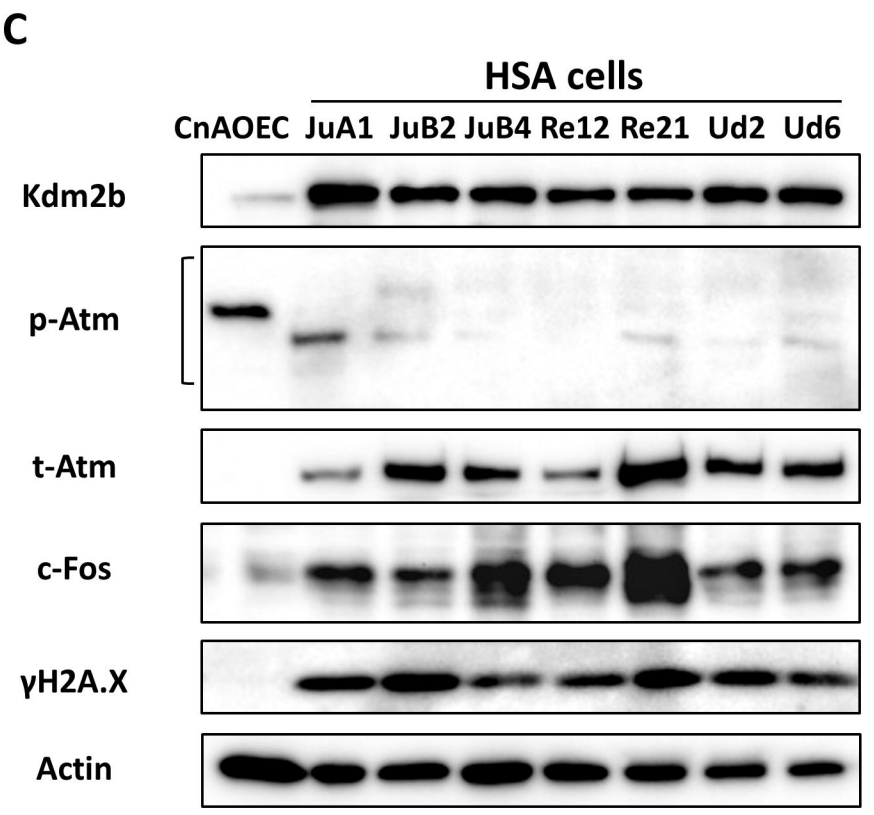

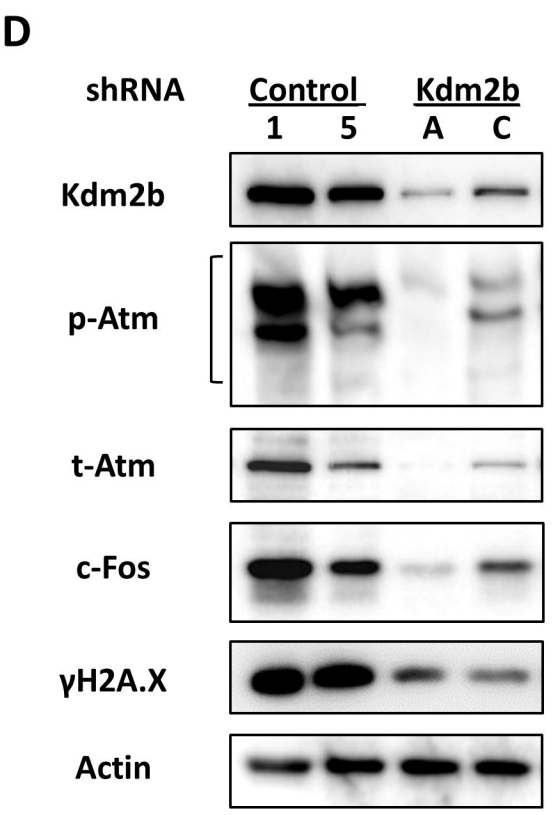

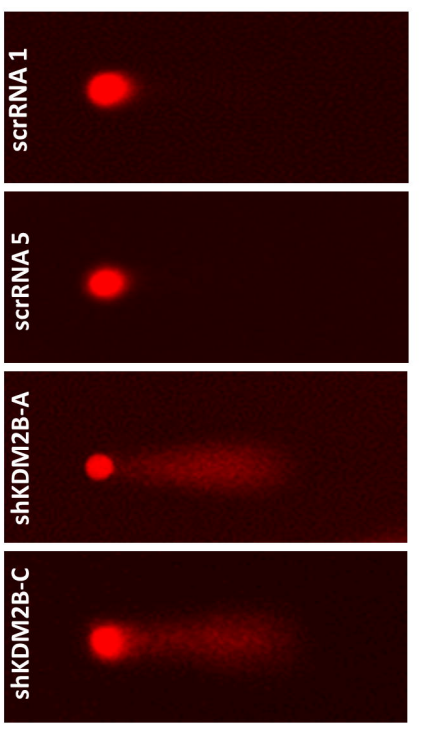

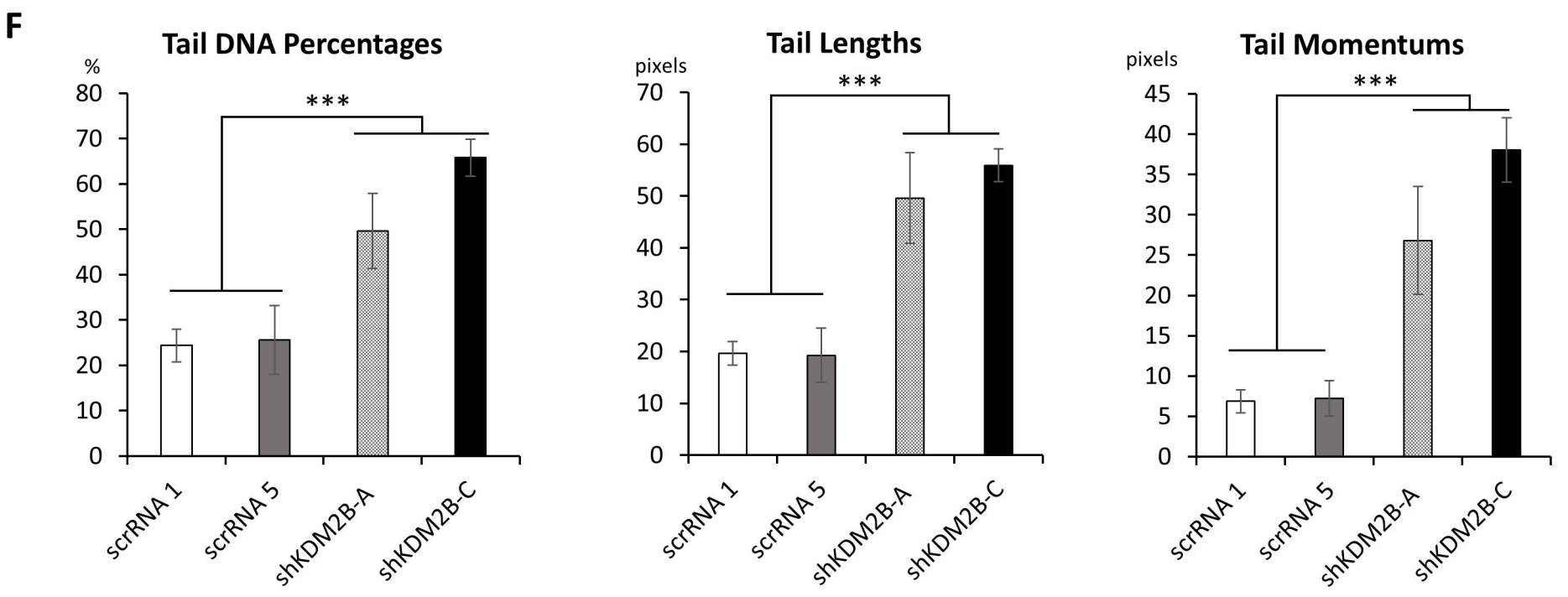

Fig. 4

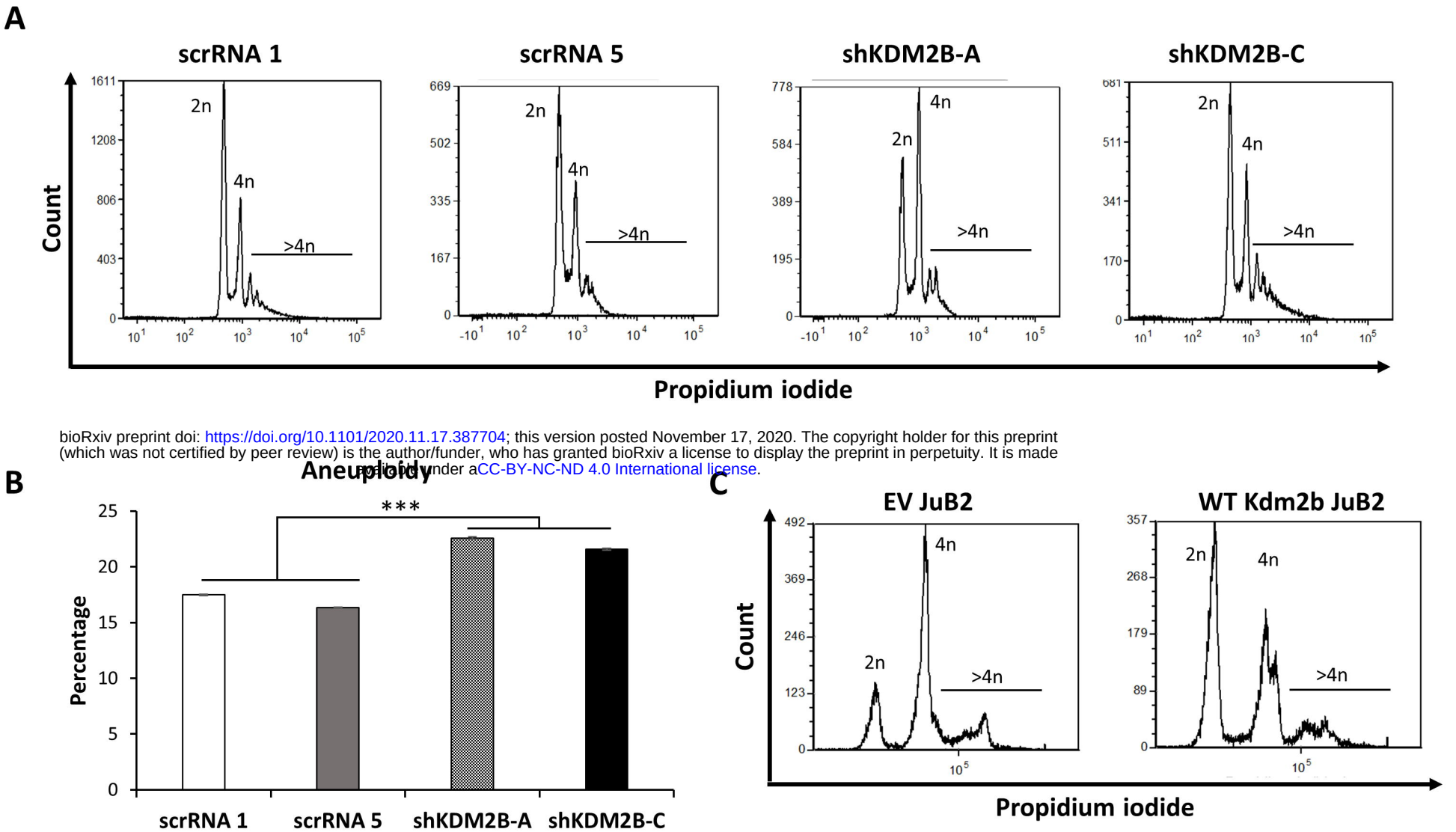

Fig. 5

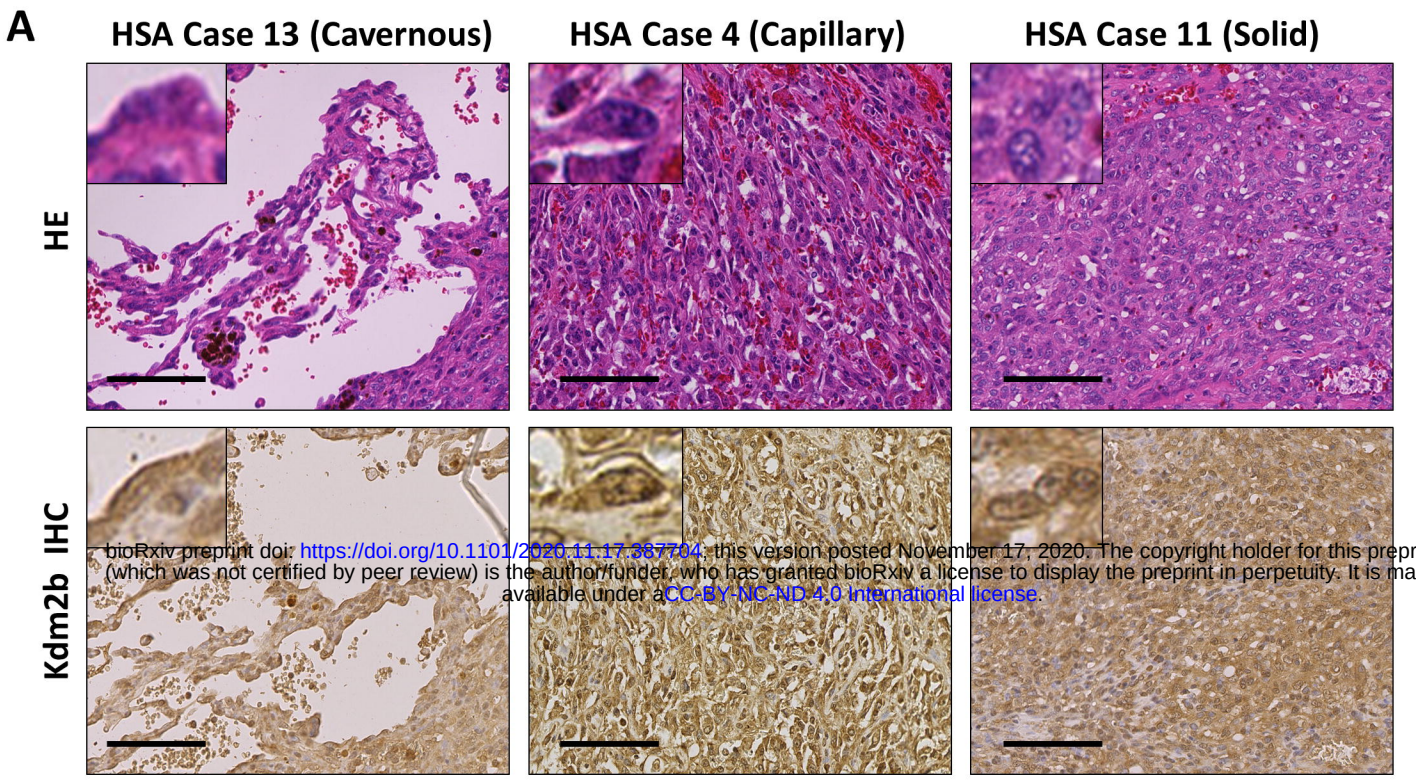

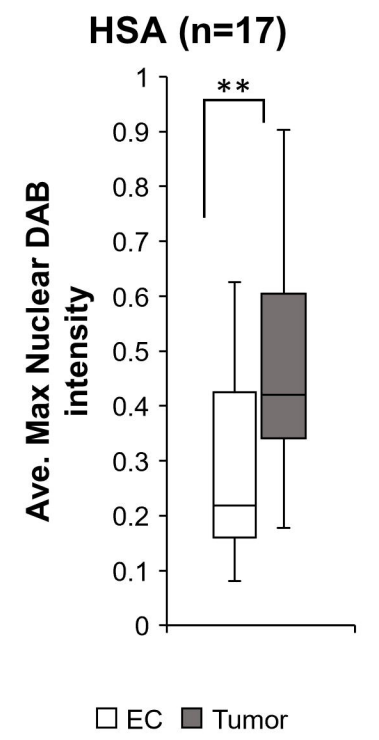

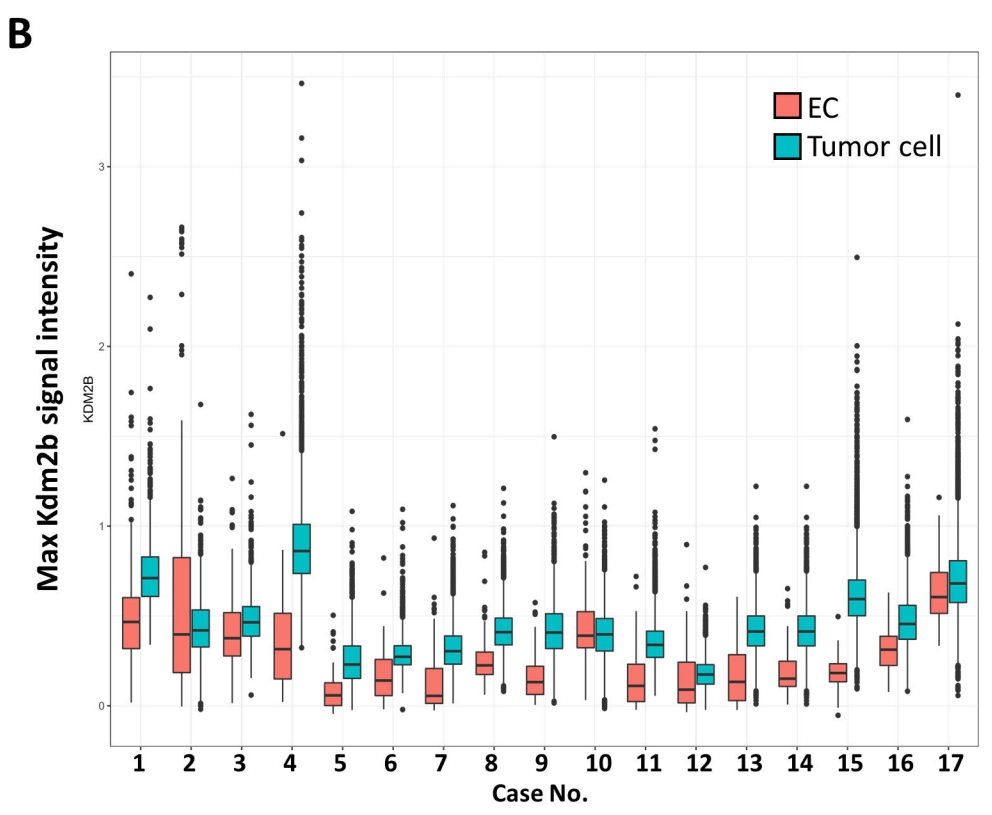

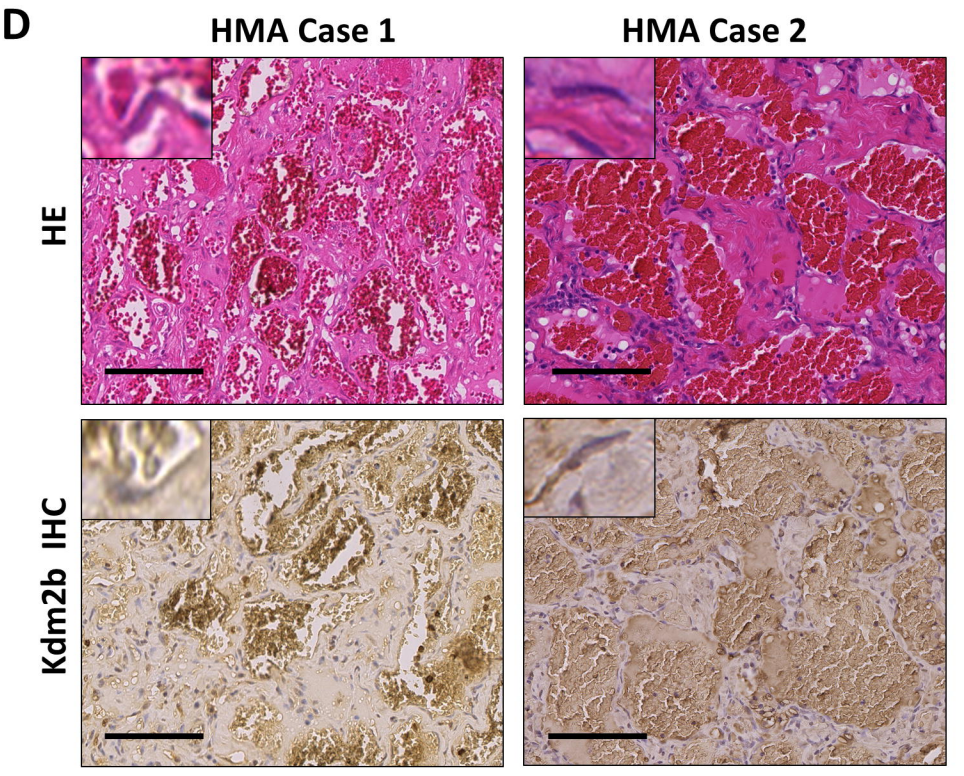

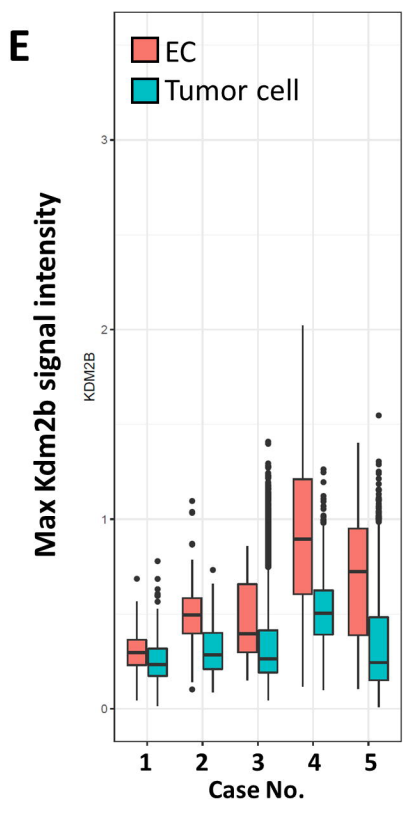

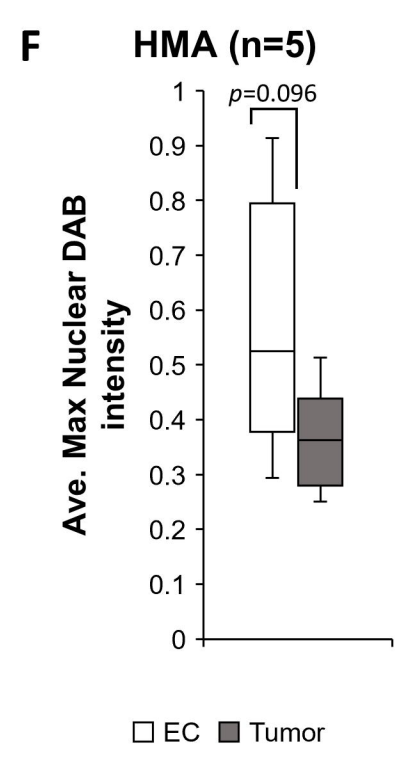

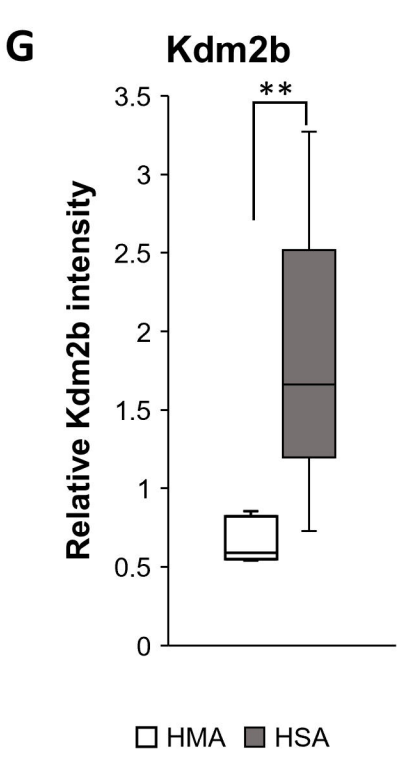

Fig. 6

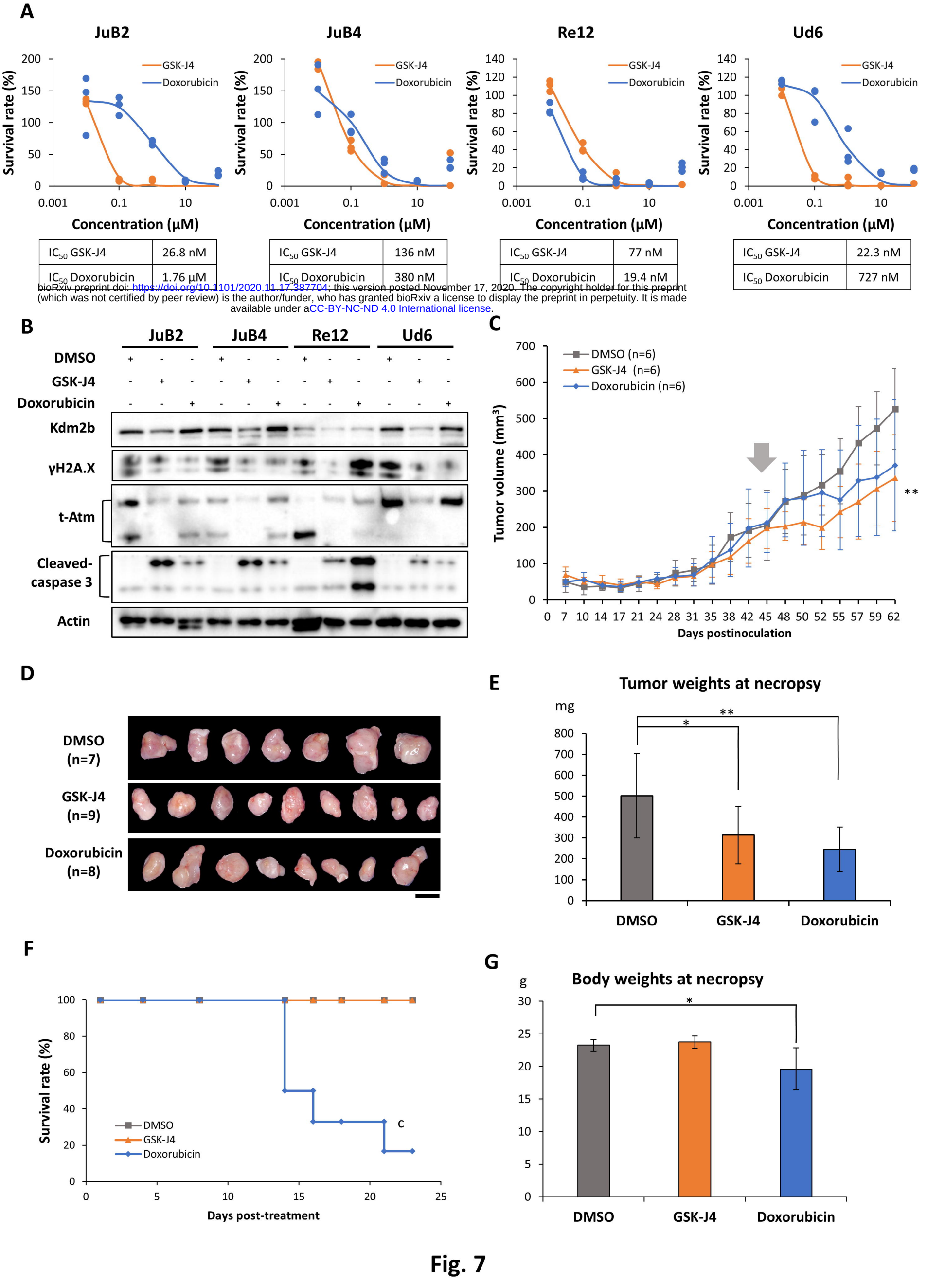

Fig. 7